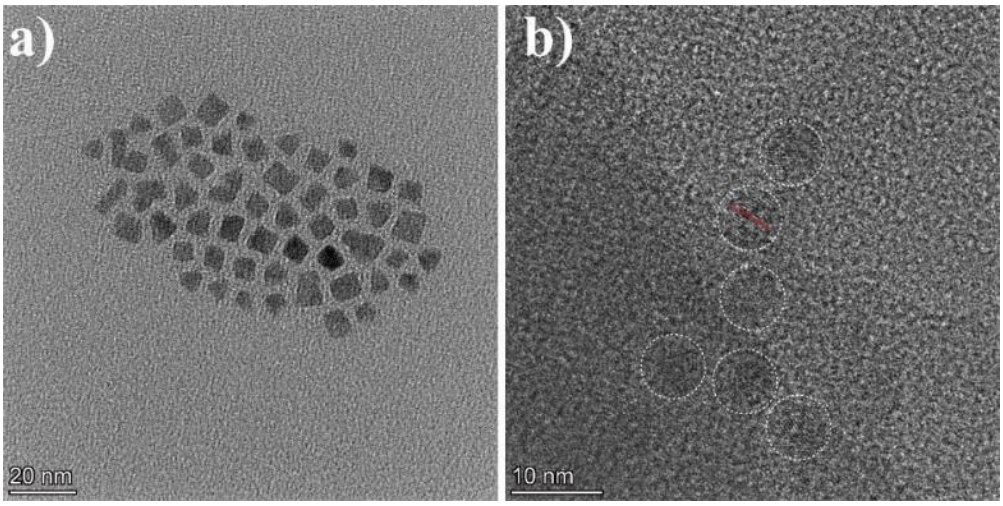

Figure S1. TEM images of oil-soluble red emitting CdSe/ZnS QDs.

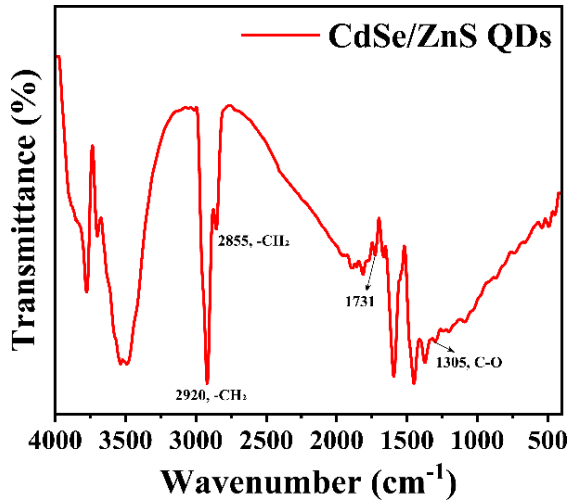

Figure S2. FT-IR spectra of oil-soluble red emitting CdSe/ZnS QDs.

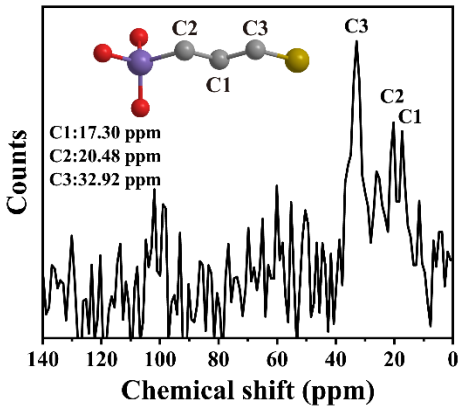

Figure S3. Solid-state ^{13}C CP/MAS NMR spectrum of SH-MF NFs. (The inset is the schematic diagrams of 3-MPTMS).

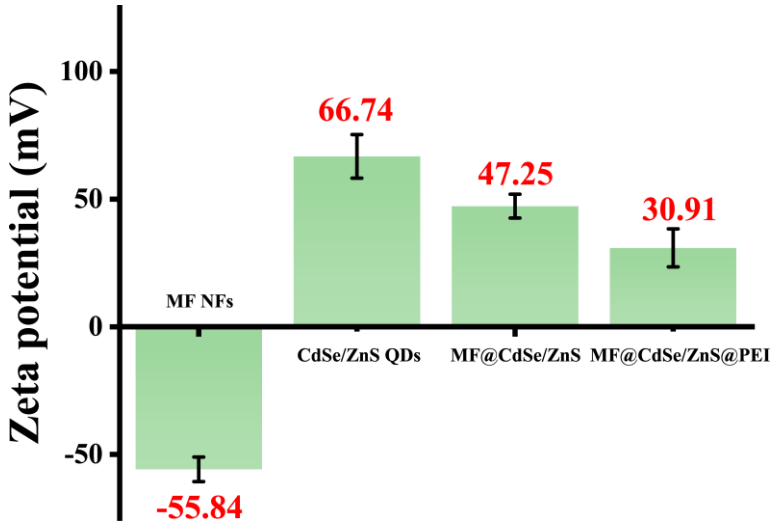

Figure S4. ζ-potential results of MF NFs, hydrophobic CdSe/ZnS QDs, MF@CdSe/ZnS, and MF@CdSe/ZnS@PEI NFs.

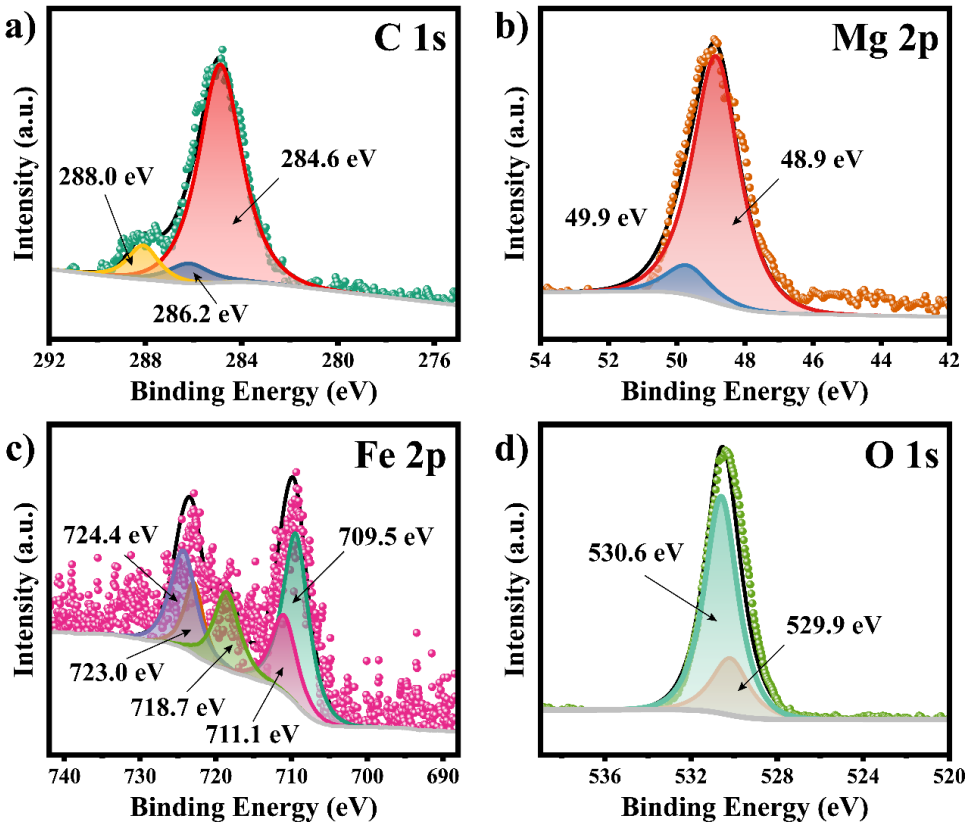

Figure S5. XPS spectra of (a) C 1s, (b) Mg 2p, (c) Fe 2p, and (d) O 1s of MF NFs.

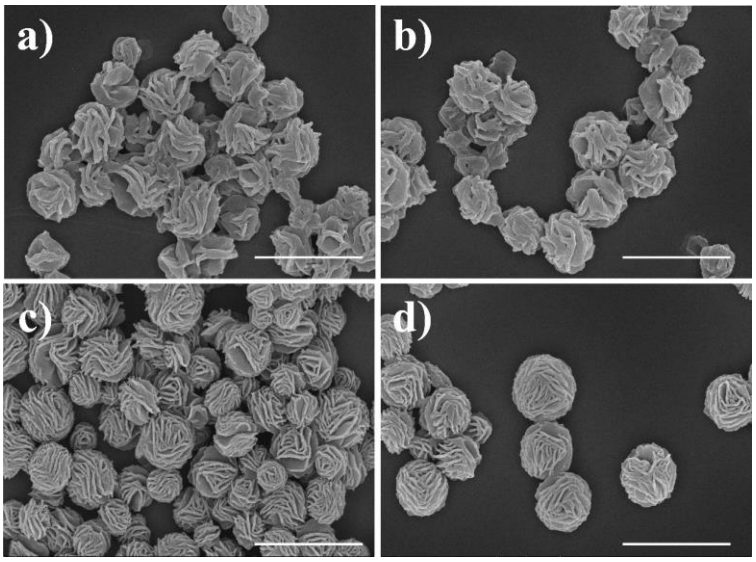

Figure S6. MF@CdSe/ZnS NFs coated with different concentrations of branched PEI (concentrations of a-d are 5, 1, 0.5, 0.1 mg/mL in order, the scale bar in the figures is 500 nm).

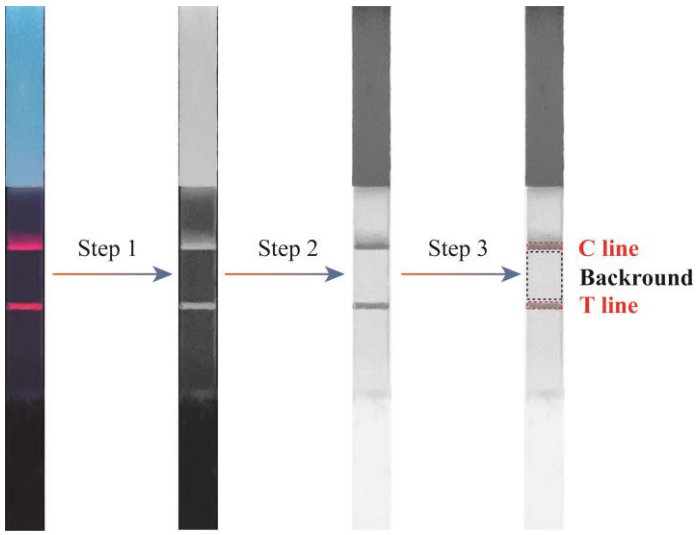

Figure S7. Image processing procedures of MF@CdSe/ZnS@PEI-ICTS. Step 1: convert the photo taken by the mobile phone into an 8-bit grayscale image. Step 2: obtain the inverse image of the grayscale image by using the "Invert" option. Step 3: define the average intensity of the T-line, C-line, and background regions in the inverse image.

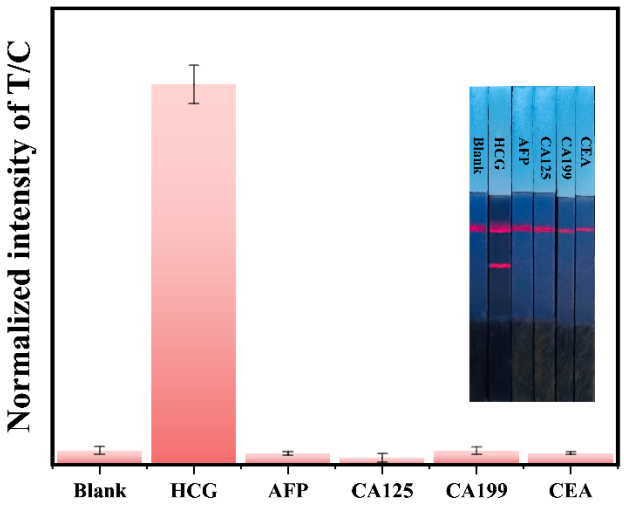

Figure S8. Cross-reactivity of MF@CdSe/ZnS@PEI-ICTS for different biomarkers.

Table S1. Recovery efficiency and coefficient of variation (CV) for the MF@CdSe/ZnS@PEI-ICTS for HCG (mIU/mL) to be detected in human serum samples (n = 3).

Biomarker	Added	Found	Recovery rate (%)	CV (%)
HCG	100	90.48 ± 0.27	90.48	7.24
	50	46.79 ± 0.83	93.58	3.66
	10	11.61 ± 0.14	116.1	12.91

Table S2. Summary of HCG detection with some different detection methods.

Methods	Limit of Detections (mIU/mL)
Electrochemiluminescence immunoassay	3×10^{-4} [1]
Photothermal immunoassay	5.8×10^{-3} [2]
Lateral flow immunoassay	3 [3]
Lateral flow immunoassay	0.22 [4]
Lateral flow immunoassay	1 [5]
Electrochemical Immunosensors	1.67×10^{-4} [6]
MF@CdSe/ZnS@PEI-ICTS (this work)	0.1

References

1. Zhang, A.; Guo, W.; Ke, H.; Zhang, X.; Zhang, H.; Huang, C.; Yang, D.; Jia, N.; Cui, D. Sandwich-format ECL immunosensor based on Au star@BSA-Luminol nanocomposites for determination of human chorionic gonadotropin. *Biosensors and Bioelectronics* **2018**, *101*, 219-226, doi:https://doi.org/10.1016/j.bios.2017.10.040.
2. Hong, G.; Zhang, D.; He, Y.; Yang, Y.; Chen, P.; Yang, H.; Zhou, Z.; Liu, Y.; Wang, Y. New photothermal immunoassay of human chorionic gonadotropin using Prussian blue nanoparticle-based photothermal conversion. *Analytical and Bioanalytical Chemistry* **2019**, *411*, 6837-6845, doi:10.1007/s00216-019-02049-w.
3. Zhang, T.; Wang, H.-B.; Zhong, Z.-T.; Li, C.-Q.; Chen, W.; Liu, B.; Zhao, Y.-D. A smartphone-based rapid quantitative detection platform for lateral flow strip of human chorionic gonadotropin with optimized image algorithm. *Microchem. J.* **2020**, *157*, 105038, doi:https://doi.org/10.1016/j.microc.2020.105038.
4. Wang, X.; Xue, C.-H.; Yang, D.; Jia, S.-T.; Ding, Y.-R.; Lei, L.; Gao, K.-Y.; Jia, T.-T. Modification of a nitrocellulose membrane with nanofibers for sensitivity enhancement in lateral flow test strips. *RSC Advances* **2021**, *11*, 26493-26501, doi:10.1039/D1RA04369B.
5. Danthanarayana, A.N.; Finley, E.; Vu, B.; Kourentzi, K.; Willson, R.C.; Brgoch, J. A multicolor multiplex lateral flow assay for high-sensitivity analyte detection using persistent luminescent nanophosphors. *Analytical Methods* **2020**, *12*, 272-280, doi:10.1039/C9AY02247C.
6. Liang, H.; Ning, G.; Wang, L.; Li, C.; Zheng, J.; Zeng, J.; Zhao, H.; Li, C.-P. Covalent Framework Particles Modified with MnO2 Nanosheets and Au Nanoparticles as Electrochemical Immunosensors for Human Chorionic Gonadotropin. *ACS Applied Nano Materials* **2021**, *4*, 4593-4601, doi:10.1021/acsanm.1c00199.